RSC Advances

PAPER

View Article Online
View Journal | View Issue

Cite this: *RSC Adv.*, 2022, **12**, 24670

Postsynthetic of MIL-101-NH_2 MOFs supported on PVDF membrane for REEs recovery from waste phosphor

Wei Qin,[a] Along Yu,[a] Xue Han,[a] Junwei Wang,*[a] Jiayin Sun,[a] Jianli Zhang[b] and Yaqing Weng[c]

With the increasing demand for rare earth elements (REEs) due to their wide application in high technology, their recovery and separation from waste sources has gradually come onto the agenda. Herein, a new kind of MIL-101-NH_2 (M1N) MOF functionalized with diethanol anhydride (DGA) incorporated into a polyvinylidene fluoride (PVDF) membrane (DGA-M1N@PVDF) has been fabricated for the sorption of REEs from a simulated acid leaching solution of waste phosphor, which contains a large amount of REEs. FTIR, TGA, XRD, fluorescence spectra and XPS analysis were used to characterize the synthesized composite membrane. Batch tests were employed to determine the optimal sorption conditions for Y and Eu adsorbed on DGA-M1N@PVDF adsorbent, such as pH (1–5), content of M1N MOFs (0–40 wt%), contact time (10–180 min) and ion concentration (0–20 mg L^{-1}). Maximum adsorption capacities for Y and Eu on DGA-M1N@PVDF reached 991.7 μg g^{-1} and 98.76 μg g^{-1} for trace REE solution, respectively. Moreover, a pseudo-second-order kinetic model accurately described the sorption process, and the plotted isothermal data indicated that the Langmuir model was more suitable than the Freundlich model for Y and Eu sorption with monolayer and chemical adsorption. Meanwhile, FTIR and XPS analyses revealed that the Y and Eu adsorption on the DGA-M1N@PVDF composite membrane was mainly caused by the N and O atoms of the –CONH or –COOH groups coordinated with metal ions. Furthermore, after five cycles, the recovery efficiency by DGA-M1N@PVDF for REEs remains above 82% and the XRD patterns were consistent with the original sample, which implied that the DGA-M1N@PVDF membrane has preferable stability, recyclability and good efficiency in REE separation from waste phosphor solutions.

Received 8th July 2022
Accepted 16th August 2022

DOI: 10.1039/d2ra04224j

rsc.li/rsc-advances

1 Introduction

Rare earth elements (REEs) are widely applied in superconductors, aerospace, electronic products, sensors and catalysis thanks to their unique electronic structure, physical and chemical performance, and excellent optical, electrical, magnetic, thermal and other properties.[1–3] With the development of the economy, there is an ever-growing demand for REEs in worldwide markets. However, REEs are scarce, unevenly distributed and non-renewable in the world. Thus, it is very important to find an effective way to separate REEs for the development of science and technology. Since phosphor powder is an important raw material of electronic light-emitting products, widely used in liquid crystal displays, diodes and fluorescent lamps, more and more waste phosphors are being produced. Waste phosphors cause environmental pollution due to a lot of heavy metals being contained in them.[4–6] Meanwhile, the waste phosphor also contains a large number of REEs, such as cerium (Ce), terbium (Tb), yttrium (Y) and europium (Eu).[7,8] Recycling REEs from waste phosphors can not only reduce environmental pollution, but also realize the secondary utilization of solid waste resources.

In recent years, traditional approaches of hydrometallurgy and pyrometallurgy have been adopted for the separation and preconcentration of REEs from waste resources,[9,10] such as co-precipitation, solvent extraction and ion-exchange.[11–13] However, most of these methods need to consume a large amount of chemical reagents, giving rise to environmental pollution, and are particularly ineffective in dealing with low-grade REEs, so their wide application is limited. Compared with traditional methods, adsorption is considered an environmentally friendly recovery method because of its low cost, non-toxicity, easy availability and recyclability.[14–18] The stability and adsorption capacity of an adsorption material mainly depend on the stability of the used material itself and on the binding affinity between functional active sites and REEs.[19,20] Nowadays, many sorbents have been employed for REE

[a]*Anhui Province Key Laboratory of Optoelectronic and Magnetism Functional Materials, Anqing Normal University, Anqing 246011, China. E-mail: wangjunweilotus@163.com; Tel: +86-556-5708017*

[b]*State Key Laboratory of High-efficiency Utilization of Coal and Green Chemical Engineering, Ningxia University, Yinchuan 750021, China*

[c]*JiangXi Academy of Sciences, Nanchang 330012, China*

separation, such as silica gel bound sorbents,[21,22] carbon nanotubes,[23] and kaolinite,[24] and ionic imprinted materials[25] and so on[26] have been employed for REE adsorption and separation.

Metal–organic frameworks (MOFs) have attracted worldwide attention due to their adjustable aperture structure, high porosity, abundant active sites and easy functionalization, and have been widely proposed for use in the application of gas separation, heterogeneous catalysis, sensors, batteries and drug delivery.[27,28] In addition, a lot of MOFs have unique bimodal pores as the structure of biological ion channels, which can accurately regulate the passage of specific target ions. But, because of the poor chemical stability of MOFs, their industrial application is restricted. To overcome this problem, the main challenge for MOFs is incorporating them into a steady substrate. Recently, MOFs loaded on films showing excellent selectivity for metal ions and high adsorption capacity have been reported.[29–32] Lu built an artificial ion channel by growing UiO-66 MOFs into a PET single channel to form a membrane, which exhibited an ultrahigh selectivity of 1590 on Li^+/Mg^{2+}.[33] Zhang[34] reported a kind of oriented UiO-67 MOFs membrane with high and fast selectivity on Li^+, and the separation factor for Li^+/Mg^{2+} reached 159.4. It was reported that MOF-808 bound with PAN over a PVDF membrane showed a high adsorption capacity for the removal of heavy metal ions from water.[35,36] All of the above results demonstrate the great potential of MOFs incorporated into membranes for ion adsorption and separation. However, the fabrication of well-grown MOF membranes for efficient ion separation remains a great challenge.

Based on the excellent stability, selectivity and recognition performance of MIL-101-NH_2 MOFs (M1N) for metal ions, this paper proposes the post-modification design and synthesis of MOFs with specific molecular recognition performance for rare earth elements contained in waste phosphors. As reported in previous studies, diglycolamic acid (DGA)[37,38] has higher distribution coefficients for actinide, lanthanide and other REE ions under highly acidic conditions. Herein, a new kind of MIL-101-NH_2 (M1N) MOF functionalized with DGA incorporated into a PVDF membrane (DGA-M1N@PVDF) has been fabricated for the green extraction and separation of Y and Eu from a simulated acid leaching solution of waste phosphor. The optimum adsorption properties of Y and Eu on this membrane were determined by batch tests. Adsorption kinetics and isotherms were used to evaluate the sorption process. FTIR and XPS analysis were employed to analyze the adsorption mechanism. Furthermore, the recycling properties of the synthesized membrane were also determined. The preparation of a MOFs-PVDF composite membrane is expected to be used in REE recovery from solid waste.

2 Experimental

2.1 Chemicals

All the chemicals, such as 2-amino-1,4-benzenedicarboxylic acid (NH_2BDC, 99%), chromium(III) nitrate nonahydrate ($Cr(NO_3)_3$, 98%) and diglycolic anhydride (DGA, 98%), were bought from Aladdin Chemical Company. Poly-*p*-phenylene terephthamide (PPA), and other reagents were bought from XiLong Scientific Company of China. Deionized water was used throughout the whole experiment, and all reagents used were analytical grade without extra purification.

2.2 Preparation of diglycolic anhydride functionalized MIL-101-NH_2 MOFs incorporated into a PVDF membrane

The preparation scheme for M1N MOFs modified with DGA incorporated into a PVDF membrane is shown Fig. 1. The preparation process is now given in detail.

2.2.1 Preparation of DGA-M1N MOFs. A solvothermal method was used to prepare M1N MOFs, as reported in ref. 39: 0.36 g of $Cr(NO_3)_3 \cdot 9H_2O$ (1.5 mmol), 0.36 g of NH_2BDC (2 mmol) and 0.2 g of NaOH (5 mmol) were blended in 15 mL of deionized water and the suspension was mixed and stirred for 0.5 h at room

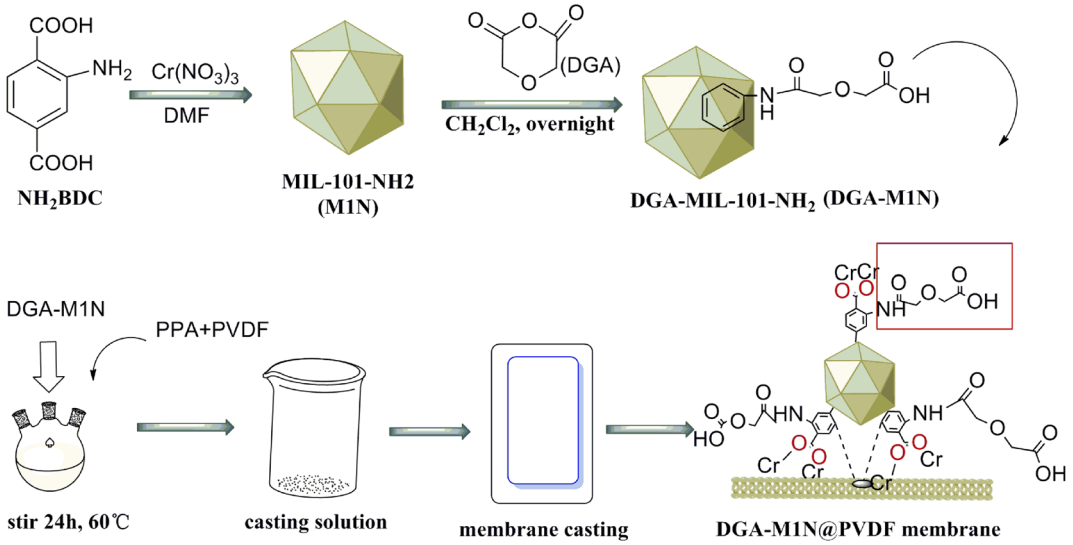

Fig. 1 Synthesis route of DGA-M1N@PVDF composite membrane.

temperature. Then, the suspension was transferred into a high-pressure reactor and kept at 150 °C for 12 h. The mixture cooled to room temperature naturally, and was then washed with DMF, ethyl alcohol and deionized water, respectively. A light-green solid product was obtained and dried in an oven at 373 K for 12 h; and the product was abbreviated as M1N MOFs.

4.0 g of M1N, 1.2 g of DGA and 20 mL of methylene chloride were blended in 250 mL three-necked bottle, and reacted at room temperature for 24 h; then, the suspension was washed with ethanol and deionized water to neutral. The product was dried in a vacuum oven at 60 °C for 12 h, and the obtained product was shortened to DGA-M1N.

2.2.2 Preparation of DGA-M1N@PVDF composite membrane. A certain amount of PVDF, 6% PPA, DGA-M1N material and 20 mL of DMF were mixed and stirred in a three-necked bottle at 60 °C for 24 h. Then, the mixed membrane precursor solution was placed in a clean beaker to debubble. After defoaming, the casting liquid was evenly scraped and coated on a dry glass plate with a casting device, and the glass plate was smoothly placed in deionized water. After the membrane had automatically fallen off from the glass plate, the glass plate was removed, and the fallen membrane was left in water for 48 h, and the composite DGA-M1N@PVDF membrane was naturally dried and obtained.

2.3 REE recovery from simulated acid leaching solution of waste phosphor

In the study, the concentration of REE solution was prepared by simulating the acid leaching solution of waste phosphor, as reported in a reference from our laboratory, where the trace concentrations of Y and Eu were 2.491 mg L^{-1} and 0.168 mg L^{-1}.[40] Batch sorption tests of Y and Eu on the DGA-M1N@PVDF composite membrane were performed, and the effect of solution acidity (pH from 0.5 to 3.0), contact time (10–120 min), initial concentration of ions and temperature from 20 to 80 °C were measured. In a typical test, 50 mg of synthesized DGA-M1N@PVDF composite membrane was suspended in 10 mL of REE simulated solution. The suspension was shaken at 25 °C for a certain time, then filtrated and the ion concentration was examined by ICP-AES. The adsorption capacity Q_e (μg g^{-1}) was determined with the following formula:[41]

$$Q_e = \frac{(C_0 - C_e) \times V}{W} \quad (1)$$

Here C_0 is the concentration of Y or Eu before adsorption, and C_e is the equilibrium concentration after adsorption (μg L^{-1}); V is the volume of solution (mL) used in the test; and W is the mass of DGA-M1N@PVDF (g).

2.4 Characterization

A Nicolet AVATAR 360 spectrophotometer was used to determine the FTIR spectra. SEM analysis of the surface was characterized using an FESEM microscope, Gemini 500 (Germany). XPS was measured using an AXIS Ultra DLD spectrometer. TGA was analyzed with an STA409PC. An ICP-AES (Thermo optima 8000D) was employed to examine the ion concentration.

3 Results and discussion

3.1 Characterizations of DGA-M1N@PVDF composite membrane

3.1.1 FTIR analysis. The FTIR spectra for the synthesized M1N, DGA-M1N and DGA-M1N@PVDF membrane are shown in Fig. 2. The bands at 3432 cm^{-1}, 1584 cm^{-1} and 1387 cm^{-1} of M1N (Fig. 2a) MOF are caused by N–H bending vibration, C–N stretching of aromatic amine, C=O stretching frequency of –COOH and the symmetric vibration of $-NH_2$.[42] The C–O–C stretching vibration band at 1130 cm^{-1} of DGA-M1N was compared with M1N, which indicated that M1N was successfully modified by DGA.[43] There were two obvious absorption peaks at 1180 and 1380 cm^{-1} shown as Fig. 2c, which correspond to the $-CF_2$ and $-CH_2$ groups of PVDF, respectively, implying the successful synthesis of the DGA-M1N@PVDF composite membrane. Moreover, no new peak was generated for the DGA-M1N@PVDF composite film, indicating that there was no chemical interaction between DGA-M1N and PVDF, and the MOF material was only physically loaded onto PVDF.

3.1.2 XRD and SEM characterization. As shown as Fig. 3a, the XRD patterns of DGA-M1N and DGA-M1N@PVDF were same as those of M1N without additional notable characteristic peaks, which indicated that the crystal structure of M1N was well retained during the modification process with DGA and also retained well in the process of preparing the composite membrane. The XRD patterns of DGA-M1N have the same characteristics after immersion in an aqueous solution of pH 2–12 for 24 h and the diffraction angles (2θ) of the three strong peaks in Fig. 3a and b are basically the same, which implies from Fig. 3b that DGA-M1N has good chemical stability.

In addition, SEM was employed to examine the surface morphology of DGA-M1N after being supported on a PVDF membrane. The SEM images show that a large amount of DGA-M1N (Fig. 3c) was wrapped inside in the DGA-M1N@PVDF composite membrane (Fig. 3d), and the morphology did not change, which implied that the morphology of DGA-M1N is well maintained after being supported on the PVDF membrane.

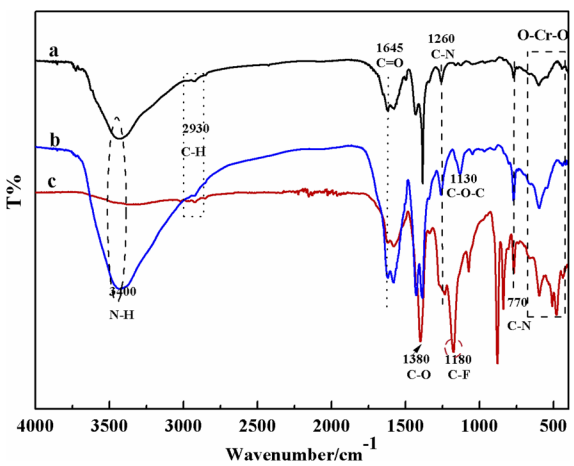

Fig. 2 FTIR analysis of the synthesized materials: (a) M1N, (b) DGA-M1N and (c) DGA-M1N@PVDF membrane.

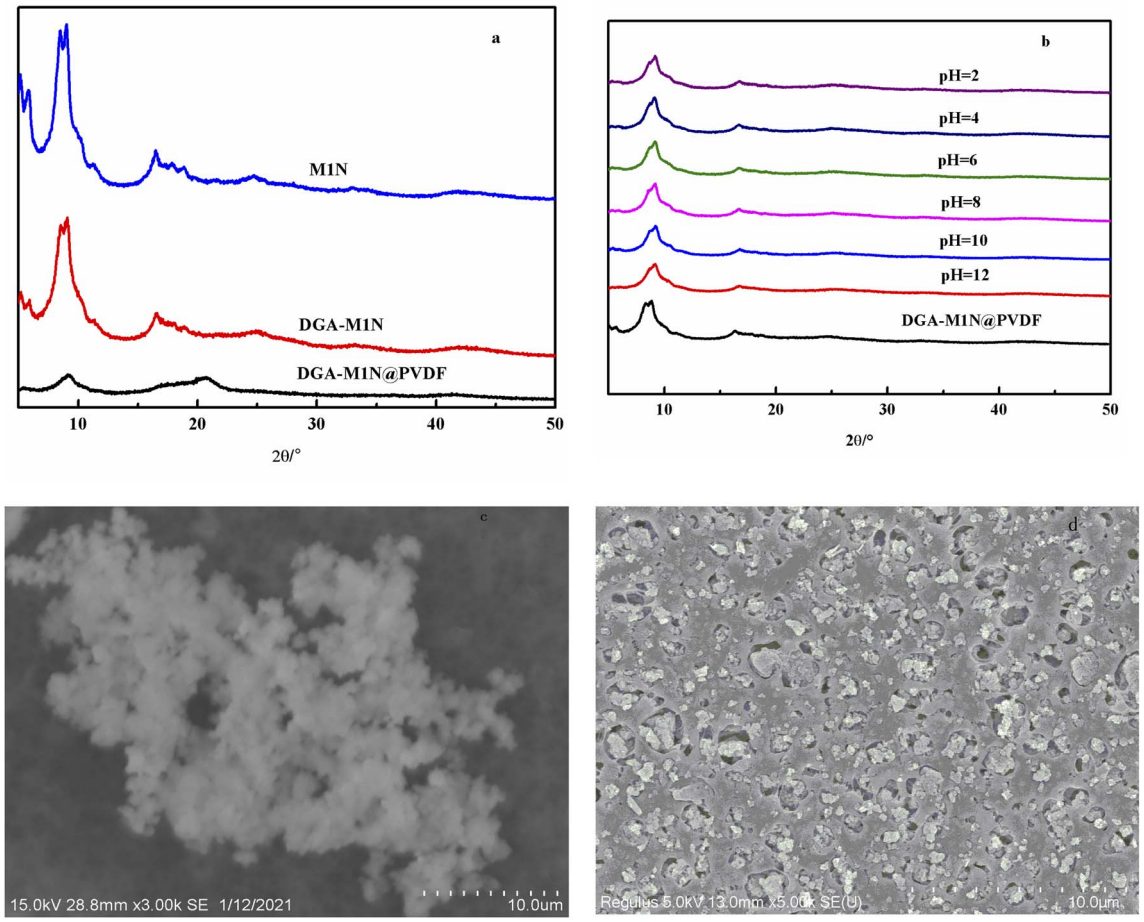

Fig. 3 XRD patterns of M1N, DGA-M1N and DGA-M1N@PVDF (a). XRD analysis of the chemical stability of DGA-M1N (b). Surface SEM images of DGA-M1N (c) and DGA-M1N@PVDF (d).

3.1.3 TGA analysis. The TGA curve of the synthesized DGA-M1N@PVDF composite membrane is shown in Fig. 4. Two stages of decomposition appear on the curve of the DGA-M1N@PVDF membrane: one weight loss from 75 to 450 °C was caused by the evaporation of residual water, while the other from 450 °C was caused by the decomposition of the membrane. When the temperature heated up to 800 °C, the weight losses of M1N (a), DGA-M1N (b) and DGA-M1N@PVDF (c) were 30.52%, 31.58% and 62.29%, respectively. By comparative analysis of the three curves, DGA-M1N was confirmed as successfully loaded on the PVDF membrane by the increasing weight loss.

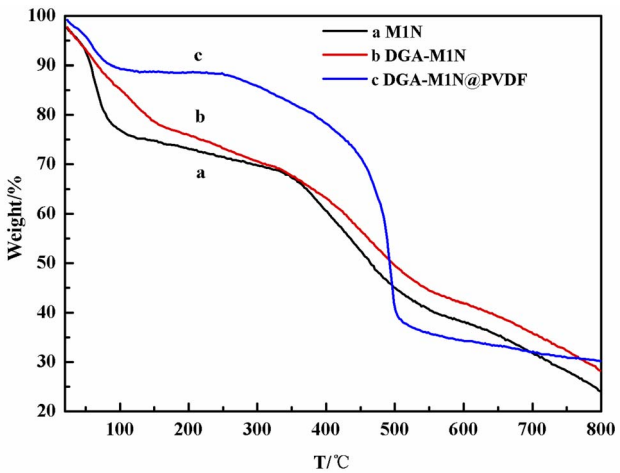

Fig. 4 TGA analysis of M1N (a), DGA-M1N (b) and DGA-M1N@PVDF (c).

3.1.4 Selectivity of the DGA-M1N@PVDF composite membrane for different ions. Furthermore, to understand the selectivity of the synthesized composite membrane for REE ions, luminescent emission spectroscopy was employed to observe the addition of K^+, Na^+, Ca^{2+}, Mg^{2+}, Cu^{2+}, Zn^{2+}, Pb^{2+}, La^{3+}, Ce^{3+}, Nd^{3+}, Y^{3+} and Eu^{3+} ions at 341 nm. From Fig. 5 we can see that among these metal ions, the addition of La^{3+} caused the maximum relative reduction in absorbance ($I_0 - I/I_0$); second was Eu^{3+}, and third was Y^{3+}. The result indicated that the DGA-M1N@PVDF composite membrane showed excellent selectivity for REEs (La^{3+}, Y^{3+} and Eu^{3+}); and the synthesized membrane showed a better separation factor for Eu^{3+} than Y^{3+}.

3.2 REE adsorption performance

3.2.1 The influence of acidity on adsorption capacity. The adsorption capacity of the DGA-M1N@PVDF composite

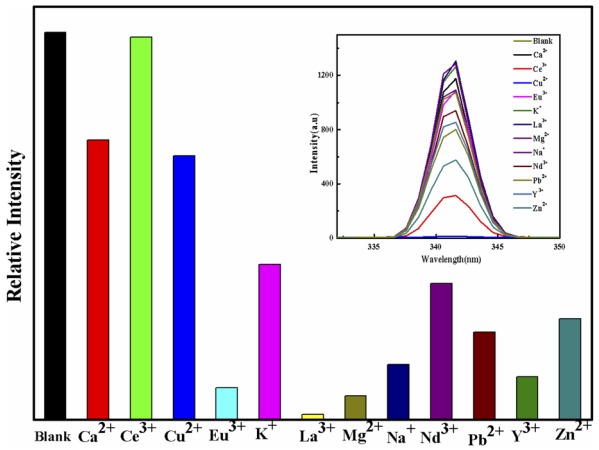

Fig. 5 Relative luminescent intensities at λ_{max} = 341 nm for DGA-M1N@PVDF upon the addition of different metal ions.

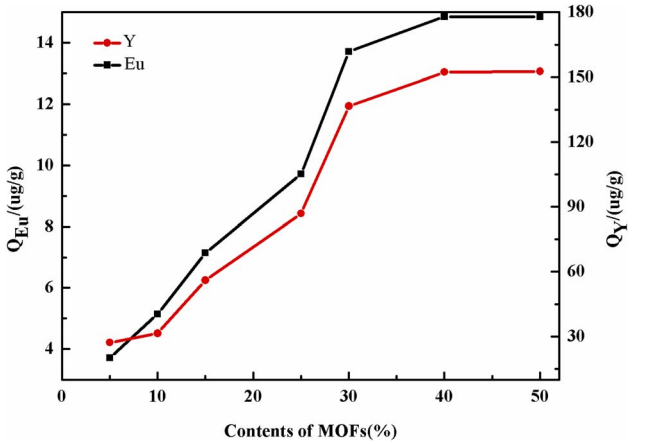

Fig. 7 The influence of different contents of DGA-M1N on the adsorption capacities for Y and Eu.

membrane on Y and Eu in the simulated solution of waste phosphor acid leaching solution rises with increasing pH, and reaches a maximum adsorption capacity when the pH is 4, as shown in Fig. 6. The adsorption capacities for Y and Eu are 136.85 μg g^{-1} and 13.33 μg g^{-1}, respectively. But, when the pH continues to increase from 4 to 5, the adsorption capacity begins to decrease, which may be caused by the hydrolysis of some Y and Eu under low acidity. The MOF materials have a certain pore size and can selectively adsorb ions of different particle sizes. The radius of the hydrated ions may increase with the hydrolysis of rare earth ions, so that the MOF pore size does not match the radius of the hydrated ions and makes them hard to adsorb, so the optimized pH is 4.

3.2.2 Effect of the content of DGA-M1N. As shown in Fig. 7, the adsorption capacity by the DGA-M1N@PVDF composite membrane for Y and Eu in the simulated solution of waste phosphor acid leaching solution increases with increasing loading contents of DGA-M1N, and reaches saturation when the loading contents reaches 40%. At this point, the maximum adsorption capacities for Y and Eu are 152.28 μg g^{-1} and 14.86 μg g^{-1} respectively. As the loading content of DGA-M1N continues to increase, the adsorption capacities of the composite membrane for Y and Eu change little, so the optimal loading content is determined to be 40%.

3.2.3 Contact time and kinetics study. As can be seen from Fig. 8, the adsorption capacities by the DGA-M1N@PVDF composite membrane for Y and Eu first increase with increasing time, reach a maximum at 120 min, and then the adsorption gradually reaches equilibrium. This may be because the adsorption occurs mainly on the film surface at the beginning, but as time increases the Y, Eu ions interact with the reactive functional groups of the composite membrane, so the adsorption capacity increases until it reaches saturation. Therefore, 120 min was selected as the optimized adsorption time, and the maximum adsorption capacities for Y and Eu reached 823.95 μg g^{-1} and 74.25 μg g^{-1}, respectively.

To further understand the adsorption mechanism, sorption kinetic models of Y and Eu ions on the DGA-M1N@PVDF membrane were established. There are usually two kinetic

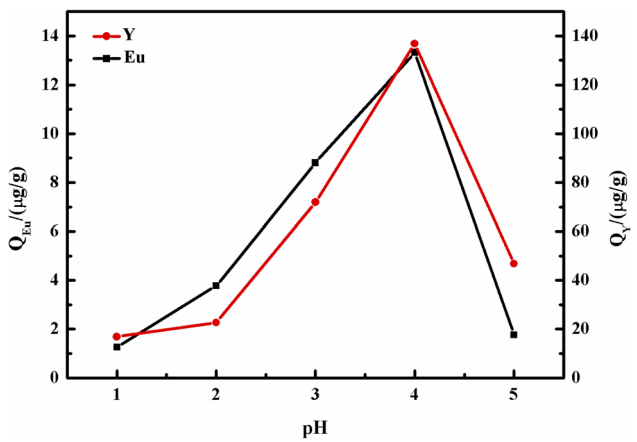

Fig. 6 The influence of different pH values on the adsorption capacities for Y and Eu.

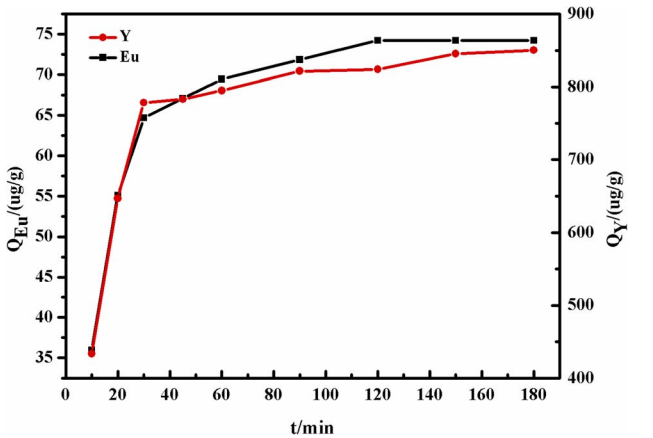

Fig. 8 The influence of different adsorption times on the adsorption capacities for Y and Eu.

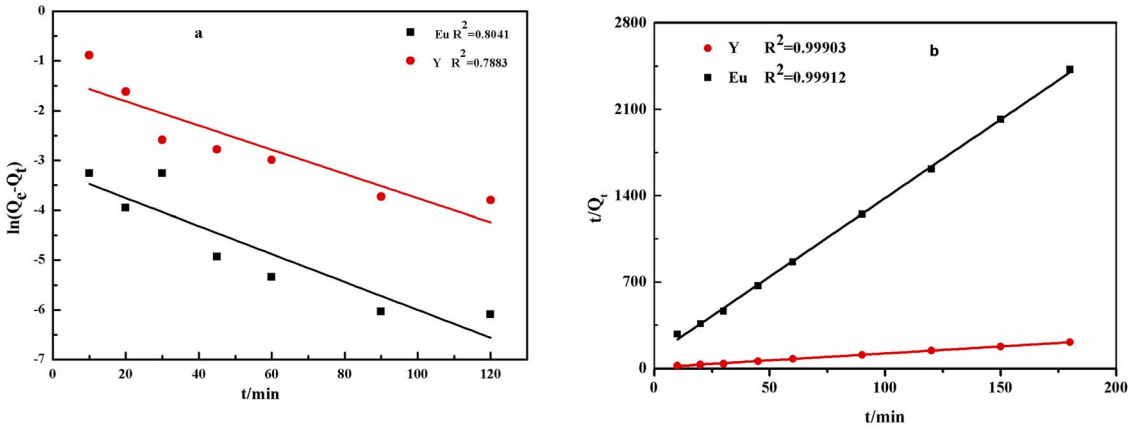

Fig. 9 (a) Pseudo-first-order kinetic fitting; (b) pseudo-second-order kinetic fitting.

Table 1 Calculated kinetic parameters of Y and Eu adsorbed on the DGA-M1N @PVDF membrane

	Parameters of pseudo-first-order				Parameters of pseudo-second-order			
	K_1 (min^{-1})	R^2	$Q_{e,cal}$ (μg g^{-1})	$Q_{e,exp}$ (μg g^{-1})	K_2 (mg g^{-1} min^{-1})	R^2	$Q_{e,cal}$ (μg g^{-1})	$Q_{e,exp}$ (μg g^{-1})
Y	−0.028	0.79	24.37	845.5	0.01	0.99	883.75	845.5
Eu	−0.024	0.80	3.75	74.25	20.33	0.99	78.42	74.25

models: one pseudo-first-order and the other pseudo-second-order,[44] as described by the following formulas:

$$-\ln(Q_e - Q_t = K_1 t - \ln Q_e \quad (2)$$

$$\frac{t}{Q_t} = \frac{1}{K_2 \times Q_e^2} + \frac{t}{Q_e} \quad (3)$$

Here t is sorption time, Q_t and Q_e are the adsorption capacities for Y and Eu at time t under equilibrium conditions; K_1 and K_2 are the rate constants of the two models. The calculated parameters of K_1, K_2, $Q_{e,cal}$ (the calculated Q_e) and R^2 (the correlation coefficient) were generated through plotting, and the results are shown in Fig. 9 and the calculated parameters are listed in Table 1.

For Y and Eu, K_1 obtained from the plotted line for the first model were −0.028 min^{-1} and −0.024 min^{-1}, and the R^2 were 0.79 and 0.80, whereas the R^2 obtained for the pseudo-second-order model was 0.99 for both ions. For the first model, the calculation results for Q_e ($Q_{e,cal}$) were very different from the experimental results ($Q_{e,exp}$), whereas, for the second model, the $Q_{e,cal}$ results were very similar to $Q_{e,exp}$. So the process of adsorbing process Y and Eu on the DGA-M1N@PVDF membrane can be better described by the pseudo-second-order models with their higher R^2. The results indicate that the decisive sorption process for Y and Eu was determined by the surface reaction, which was caused by the coordination of functional groups of the composite membrane with the rare earth elements.[45]

3.2.4 Effect of initial ion concentration and adsorption isotherms study. The changing amounts of Y and Eu adsorbed on the DGA-M1N membrane as a function of concentration in the range of 0–20 mg L^{-1} at pH 4 are shown in Fig. 10. The amounts of Y and Eu adsorbed on the DGA-M1N@PVDF composite membrane (Q_Y and Q_{Eu}) increase with increasing concentration. When the concentrations of Y and Eu reach 14.95 mg L^{-1} and 1.01 mg L^{-1}, the rate of increases of Q_e is slow, and the maximum adsorption amounts are 991.7 and 98.76 μg g^{-1} for Y and Eu, respectively. To elucidate the sorption process, the Langmuir and Freundlich models[46] (eqn (4) and (5)) were used here to deal with the data, and the calculated results are listed in Table 2.

$$\text{Langmuir}: \quad \frac{C_e}{Q_e} = \frac{1}{K_L \times Q_{max}} + \frac{C_e}{Q_{max}} \quad (4)$$

$$\text{Freundlich}: \quad \ln Q_e = \ln K_F + \frac{1}{n} \times \ln C_e \quad (5)$$

where Q_e and Q_{max} are the equilibrium and the calculated adsorption capacities (mg g^{-1}), respectively. C_e (mg L^{-1}) is the equilibrium concentration of Y or Eu. K_L (L mg^{-1}) and K_F are empirical constants.

A straight line (R^2 = 0.98) was obtained by plotting C_e/Q_e against C_e, as shown in Fig. 10 and the calculated parameters are listed in Table 2. The results implied that the Langmuir adsorption isotherm was inconsistent with good Y and Eu sorption on the DGA-M1N@PVDF composite membrane. The calculated maximum adsorption capacities (Q_{max}) were 4.5 mg g^{-1} and 0.43 mg g^{-1} for Y and Eu, respectively and the calculated constants K_L for Y and Eu are 0.02 and 0.26 L mg^{-1}. We all know that the Langmuir isotherm is employed to describe

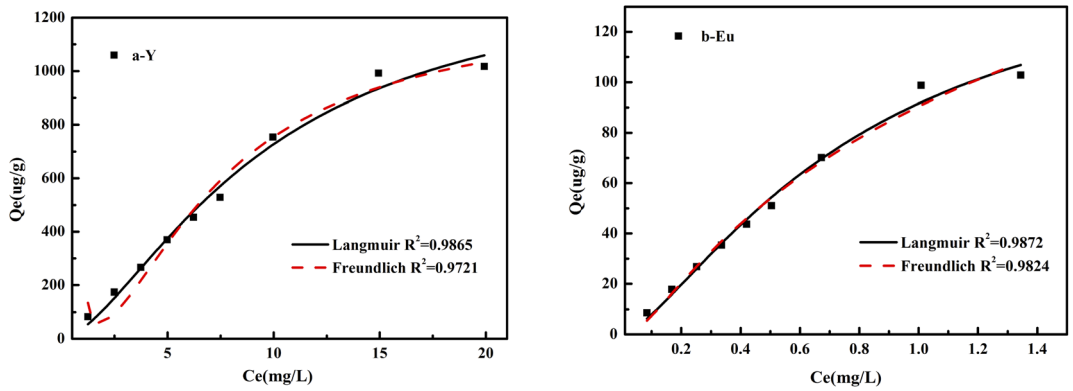

Fig. 10 Fitting diagram of Langmuir and Freundlich adsorption isotherm parameters of Y and Eu adsorbed on the DGA-M1N@PVDF composite membrane.

homogeneous sorption, and the weaker the adsorption, the smaller the K_L. So it could be inferred that the adsorption of Eu on DGA-M1N@PVDF was stronger than that of Y, and the sorption well belongs to monolayer adsorption. Although the quality of Langmuir and Freundlich fitting is very similar, the Langmuir model exhibits a better match with the data (R^2 = 0.98) than the Freundlich model, which implies that the Langmuir adsorption isotherm was consistent with Y and Eu sorption on the DGA-M1N@PVDF composite membrane. In a comparison of the adsorption capacity for Y and Eu with other sorbents in the ref. 47–50, the synthesized DGA-M1N@PVDF composite membrane displayed good adsorption capacity for Y and Eu in the acid leaching simulation solution with a trace of waste phosphor. Thus, it can be concluded that DGA-M1N@PVDF is a favorable sorbent for REEs.

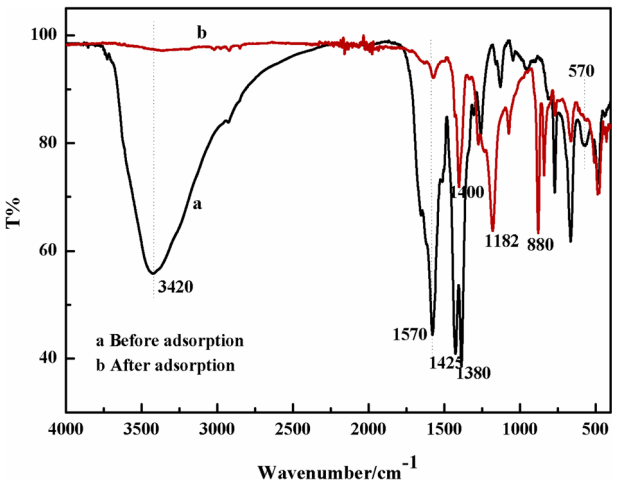

Fig. 11 FTIR analysis of the synthesized membrane before and after adsorption.

3.3 Adsorption mechanism of REEs on the DGA-M1N@PVDF membrane

3.3.1 FTIR study. To evaluate the sorption mechanism of REEs on the DGA-M1N@PVDF membrane, FTIR was employed to examine the interaction between REEs and DGA-M1N@PVDF. The FTIR spectra of DGA-M1N@PVDF before and after loading with Y and Eu are listed in Fig. 11. Peaks at 880 and 1182 cm^{-1} were apparent after adsorption, which might be caused by Y–N and Eu–N stretching vibration, and implied that the REEs were connected with DGA-M1N@PVDF through a coordination reaction. Furthermore, the fact that the peak at 3420 cm^{-1} disappeared after adsorption suggested that Y and Eu are connected with the membrane through REEs–O interaction.

3.3.2 XPS study. To further identify the participation of REEs coordinated with DGA-M1N@PVDF, XPS was also employed to analyze the membrane before and after adsorption, and the detailed results are shown in Fig. 12. The total scan spectra of DGA-M1N@PVDF before and after adsorption, and the signals of the main elements, such as C 1s, N 1s, O 1s, Y 3d and Eu 3d, were recorded in the experiment. It is apparent that weak signals of Y 3d and Eu 3d appeared at 161.8eV and 1145.7eV after adsorption, as shown in Fig. 12a, which clearly indicated the sorption of Y and Eu on DGA-M1N@PVDF after the membrane had been equilibrated in the mixture solution. To further investigate the binding states of ions with the membrane, the fitted peaks of O 1s and N 1s were obtained. As can be seen from Fig. 12b, the O 1s spectrum was fitted into

Table 2 Langmuir and Freundlich adsorption isotherm parameters for Y and Eu adsorption by the composite membrane

	Langmuir				Freundlich		
	Q_e (mg g^{-1})	Q_{max} (mg g^{-1})	K_L (L mg^{-1})	R^2	K_F [$L^{1/n}$ $mg^{(1-1/n)}$ g^{-1}]	n	R^2
Y	0.99	4.50	0.02	0.98	0.07	1.06	0.97
Eu	0.10	0.43	0.26	0.98	0.09	1.08	0.98

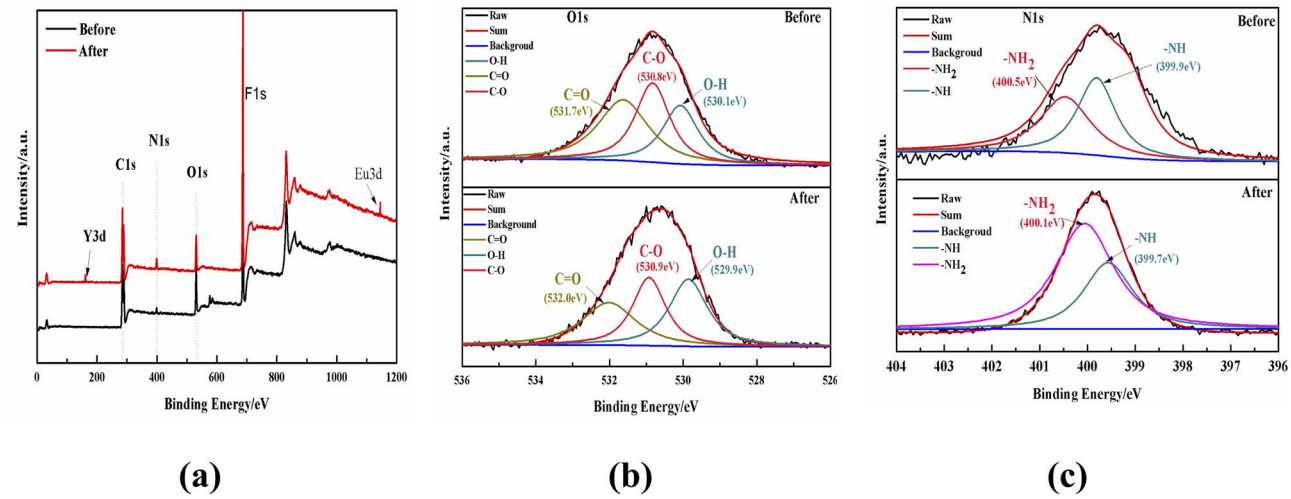

Fig. 12 XPS spectra of the DGA-M1N@PVDF membrane before and after adsorption, where (a) shows the total XPS analysis before and after sorption, (b) shows the XPS analysis of O 1s, and (c) shows the analysis of N 1s before and after sorption.

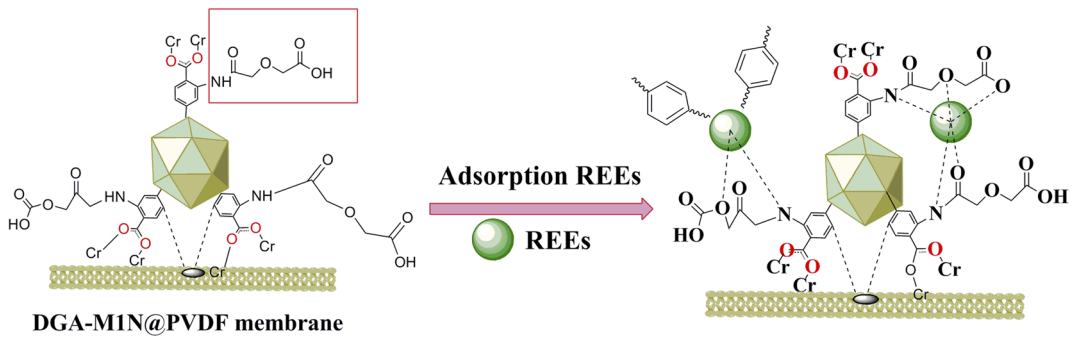

Fig. 13 Proposed binding mechanism of the DGA-M1N@PVDF composite membrane with REE metal ions.

three peaks and the binding energies at 530.1, 530.8 and 531.7 eV were further assigned to O–H, C–O and C=O species before sorption, whereas the binding energies of these species shifted to 529.9, 530.9 and 532.0 eV after adsorption, respectively.[51] The peaks of the N 1s spectrum (Fig. 12c) were fitted into two peaks for –NH, and $-NH_2$ species, and the binding energies transferred from 399.9 to 399.7 eV and from 400.5 to 400.1 eV after absorption respectively, which implied

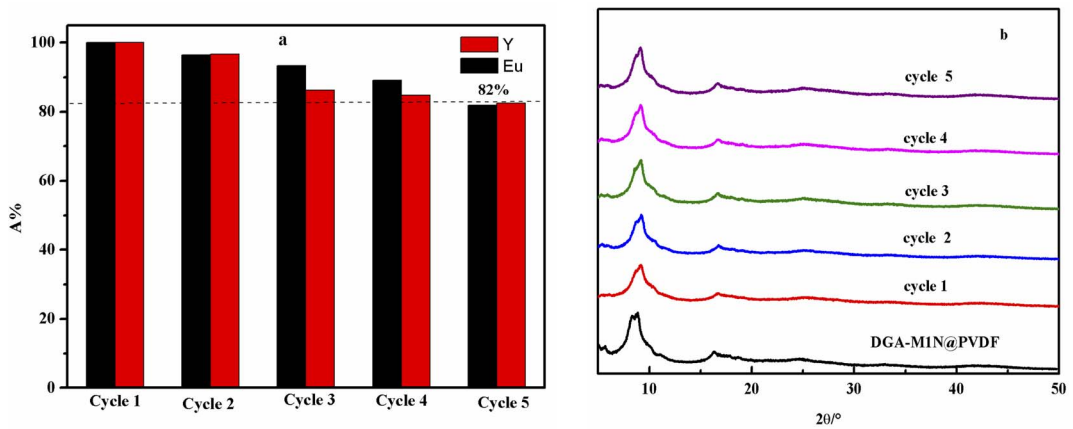

Fig. 14 The regeneration of the DGA-M1N@PVDF membrane for Y and Eu (a) and XRD analysis of the chemical stability of DGA-M1N@PVDF after five cycles of reuse (b).

that the N atoms in the –NH and $–NH_2$ groups were coordinated with the REEs during the sorption process, thus causing a higher binding energy transfer.[52] In terms of the above analyses, it can be concluded that the adsorption mechanism of the DGA-M1N@PVDF membrane with Y and Eu was mainly caused by the chelation of N and O elements of $–CONH_2$, –COOH, and $–NH_2$ groups with metal ions to form a metal complex. According to the FTIR and XPS analyses, a sorption mechanism between DGA-M1N@PVDF and Y or Eu was deduced and is shown in Fig. 13.

3.4 Reusability studies

The efficient recycling performance of a composite membrane is important for evaluating its economic and practical applications. The experimental regeneration process was tested as follows: 50 mg of DGA-M1N@PVDF membrane and 10 mL of simulated acid leaching solution were mixed and shaken for 120 min to reach adsorption equilibrium. Then, the solution was filtered, the filtrate was collected and the concentration measured by ICP-AES. Then, the membrane was soaked in HCl solution and washed until it was neutral and dried for reuse. The above steps were repeated five times, and the results are shown in Fig. 14. After five cycles of reuse, the adsorption of Y and Eu on the synthesized membrane was still more than 82%, and the diffraction peaks of the XRD pattern were still intact. That is to say, the prepared DGA-M1N@PVDF membrane shows good recycling performance for rare earth elements.

4 Conclusions

The present study has reported that a new kind of composite membrane was prepared by diethanol anhydride (DGA) functionalized on MIL-101-NH_2 MOFs incorporated into PVDF (DGA-M1N@PVDF), which was employed to separate REEs from a simulated acid leaching solution of waste phosphor. Luminescent emission spectroscopy indicated that the synthesized membrane showed good selectivity for REEs, such as Y and Eu. Adsorption tests showed that the maximum adsorptions of DGA-M1N@PVDF on Y and Eu were up to 991.7 μg g^{-1} and 98.76 μg g^{-1} in simulated acid leaching solution with a trace of waste phosphor, respectively. Furthermore, the pseudo-first-order model with a rate-controlling step was established by kinetic data analyses. And the Langmuir model was much more suitable than the Freundlich model with a monolayer adsorption process for Y and Eu. FTIR and XPS analyses indicated that the adsorption of Y and Eu on DGA-M1N@PVDF was mainly induced by chemical coordination of N and O atoms of $–CONH_2$, –COOH and $–NH_2$ groups with REEs to form a metal complex. Moreover, the recovery efficiency of DGA-M1N@PVDF for REEs remains above 82% after five cycles and the XRD patterns were still well preserved, which indicated that the synthesized membrane was a favorable sorbent for REE recycling.

Conflicts of interest

There are no conflicts to declare.

Acknowledgements

Thanks for the supports of the National Natural Science Foundation of China (51404014 and 51604129), Foundation of State Key Laboratory of High efficiency Utilization of Coal and Green Chemical Engineering (2019-KF-31, 2020-KF-28), the Natural Science Foundation of Anhui Colleges and Universities (KJ2020A0494), Foundation of Anhui Provincial Laboratory of Optoelectronic and Magnetism Functional Materials (ZD2020004), Foundation of Natural Science of Anhui Province (2008085QB55).

References

1 S. Massari and M. Ruberti, Rare earth elements as critical raw materials: focus on international markets and future strategies, *Resour. Policy*, 2013, **38**, 36–43.
2 S. M. Ramay, A. Mahmood, H. M. Ghaithan, N. S. Al-Zayed, A. Aslam, A. Murtaza, N. Ahmad, S. A. Siddiqid and M. Saleem, Magnetron sputtered Dy_2O_3 with chromium and copper contents for antireflective thin films with enhanced absorption, *J. Rare Earths*, 2019, **37**, 989–994.
3 H. Y. Zhao, J. L. Xia, D. D. Yin, M. Luo, C. H. Yan and Y. P. Du, Rare earth incorporated electrode materials for advanced energy storage, *Coord. Chem. Rev.*, 2019, **390**, 32–49.
4 A. Lucas and R. Emery, Assessing occupational mercury exposures during the onsite processing of spent fluorescent lamps, *J. Environ. Health*, 2006, **68**(30–4), 40–45.
5 Y. Hu and H. Cheng, Mercury risk from fluorescent lamps in China: current status and future perspective, *Environ. Int.*, 2012, **44**, 141–150.
6 D. D. Shao, S. C. Wu, P. Liang, Y. Kang, W. J. Fu, K. L. Zhao, Z. H. Cao and M. H. Wong, A human health risk assessment of mercury species in soil and food around compact fluorescent lamp factories in Zhejiang Province, PR China, *J. Hazard. Mater.*, 2012, **221–222**, 28–34.
7 F. Yang, F. Kubota, Y. Baba and N. Kamiya, Selective extraction and recovery of rare earth metals from phosphor powders in waste fluorescent lamps using an ionic liquid system, *J. Hazard. Mater.*, 2013, **254–255**, 79–88.
8 H. L. Yang, W. Wang, H. M. Cui, D. L. Zhang, Y. Liu and J. Chen, Recovery of rare earth elements from simulated fluorescent powder using bifunctional ionic liquid extractants (Bif-ILEs), *J. Chem. Technol. Biotechnol.*, 2012, **87**, 198–205.
9 K. Binnemans, P. T. Jones, B. Blanpain, T. V. Gerven, *et al.*, Recycling of rare earths: A critical review, *J. Cleaner Prod.*, 2013, **51**, 1–22.
10 Y. Bian, S. Guo, L. Jiang, J. Liu, *et al.*, Recovery of rare earth elements from NdFeB magnet by VIM-HMS method, *ACS Sustainable Chem. Eng.*, 2016, **4**, 810–818.
11 P. Chen, F. Yang, Q. Liao, Z. Zhao, *et al.*, Recycling and separation of rare earth resources lutetium from LYSO scraps using the diglycol amic acid functional XAD-type resin, *Waste Manage.*, 2017, **62**, 222–228.
12 C. Tunsu, J. B. Lapp, C. Ekberg and T. Retegan, Selective separation of yttrium and europium using Cyanex 572 for

applications in fluorescent lamp waste processing, *Hydrometallurgy*, 2016, **166**, 98–106.

13 D. Depuydt, V. D. B. Arne, W. Dehaen and K. Binnemans, Metal extraction with a short-chain imidazolium nitrate ionic liquid, *Chem. Commun.*, 2017, **53**, 5271–5274.

14 H. Moriwaki, R. Masuda, Y. Yamazaki, K. Horiuchi, *et al.*, Application of freeze-dried powders of genetically engineered microbial strains as adsorbents for rare earth metal ions, *ACS Appl. Mater. Interfaces*, 2016, **40**, 26524–26531.

15 M. J. Page, K. Soldenhoff and M. D. Ogden, Comparative study of the application of chelating resins for rare earth recovery, *Hydrometallurgy*, 2017, **169**, 275–281.

16 J. Roosen, J. Spooren and K. Binnemans, Adsorption performance of functionalized chitosan–silica hybrid materials toward rare earths, *J. Mater. Chem. A*, 2014, **45**, 19415–19426.

17 J. A. Shusterman, H. E. Mason, J. Bowers, A. Bruchet, *et al.*, Development and testing of diglycolamide functionalized mesoporous silica for sorption of trivalent actinides and lanthanides, *ACS Appl. Mater. Interfaces*, 2015, **37**, 20591–20599.

18 R. X. Bai, F. Yang, Y. Zhang, Z. G. Zhao, *et al.*, Preparation of elastic diglycolamic-acid modified chitosan sponges and their application to recycling of rare-earth from waste phosphor powder, *Carbohydr. Polym.*, 2018, **190**, 255–261.

19 F. Bari, N. Begum, S. B. Jamaludin and K. Hussin, Synthesis of sol-gel silica chemically bonded with Cyanex 272 for the removal of Cu (II), Ni (II) and Zn (II), *J. Mater.Sci.*, 2009, **44**, 2628–2636.

20 A. E. Karatapanis, Y. Fiamegos and C. D. Stalikas, Silica-modified magnetic nanoparticles functionalized with cetylpyridinium bromide for the preconcentration of metals after complexation with 8-hydroxyquinoline, *Talanta*, 2011, **84**, 834–839.

21 O. Artiushenko, L. Kostenko and V. Zaitsev, Influence of competitive eluting agents on REEs recovery from silica gel adsorbent with immobilized aminodiphosphonic acid, *J. Environ. Chem. Eng.*, 2020, **4**, 103883–103891.

22 D. B. wu, Y. H. sun and Q. G. Wang, Adsorption of lanthanum (III) from aqueous solution using 2-ethylhexyl phosphonic acid mono-2-ethylhexyl ester-grafted magnetic silica nanocomposites, *J. Hazard. Mater.*, 2013, **260**, 409–419.

23 D. L. Ramasamy, V. Puhakka, B. Doshi, S. Iftekhar, *et al.*, Fabrication of carbon nanotubes reinforced silica composites with improved rare earth elementsadsorption performanc, *Chem. Eng. J.*, 2019, **365**, 291–304.

24 C. Peng, Y. Zhong, G. Wang, F. Min, *et al.*, Atomic-level insights into the adsorption of rare earth $Y(OH)_3$-nn^+ (n=1∼3) ions on kaolinite surface, *Appl. Surf. Sci.*, 2018, **511**, 367–374.

25 F. Yang, F. Kubota, Y. Baba, N. Kamiya, *et al.*, Selective extraction and recovery of rare earth metals from phosphor powders in waste fluorescent lamps using an ionic liquid system, *J. Hazard. Mater.*, 2013, **254–255**, 79–88.

26 Y. F. Wu, X. F. Xin, Q. J. Zhang, W. Wang, *et al.*, The recycling of rare earths from waste tricolor phosphors in fluorescent lamps: A review of processes and technologies, *Resour. Conserv. Recycl.*, 2014, **88**, 21–31.

27 H. L. Jiang, T. Akita, T. Ishida, M. Haruta, *et al.*, Synergistic catalysis of Au@Ag core-shell nanoparticles stabilized on metalorganic framework, *J. Am. Chem. Soc.*, 2011, **133**, 1304–1306.

28 T. K. Trung, P. Trens, N. Tanchoux, S. Bourrelly, *et al.*, Hydrocarbon adsorption in the flexible metal organic frameworks MIL-53 (Al, Cr), *J. Am. Chem. Soc.*, 2008, **130**, 16926–16932.

29 M. Bansal, B. Ram, G. S. Chauhan and A. Kaushik, l-Cysteine functionalized bagasse cellulose nanofiber for mercury (II) ions adsorption, *Int. J. Biol. Macromol.*, 2018, **112**, 728–736.

30 S. Koushkbaghi, A. Zakialamdari, M. Pishnamazi, H. F. Ramandi, M. Aliabadi and M. Irani, Aminated-Fe_3O_4 nanoparticles filled chitosan/PVA/PES dual layers nanofbrous membrane for the removal of Cr (VI) and Pb (II) ions from aqueous solutions in adsorption and membrane processes, *Chem. Eng. J.*, 2018, **337**, 169–182.

31 L. Li, F. Wang, Y. Lv, J. Liu, *et al.*, Halloysite nanotubes and Fe_3O_4 nanoparticles enhanced adsorption removal of heavy metal using electrospun membranes, *Appl. Clay Sci.*, 2018, **161**, 225–234.

32 L. R. Rad, A. Momeni, B. F. Ghazani, M. Irani, *et al.*, Removal of Ni^{2+} and Cd^{2+} ions from aqueous solutions using electrospun PVA/zeolite nanofbrous adsorbent, *Chem. Eng. J.*, 2014, **256**, 119–127.

33 J. Lu, H. C. Zhang, J. Hou, X. Y. Li, *et al.*, Efficient metal ion sieving in rectifying subnanochannels enabled by metal-organic frameworks, *Nat. Mater.*, 2020, **19**, 767–774.

34 R. M. Xu, Y. Kang, W. M. Zhang, X. W. Zhang, *et al.*, Oriented UiO-67 Metal–Organic Framework Membrane with Fast and Selective Lithium-Ion Transport, *Angew. Chem., Int. Ed.*, 2021, **60**, 1–6.

35 J. E. Efome, D. Rana, T. Matsuura and C. Q. Lan, Experiment and modeling for flux and permeate concentration of heavy metal ion in adsorptive membrane filtration using a metal-organic framework incorporated nanofbrous membrane, *Chem. Eng. J.*, 2018, **352**, 737–744.

36 J. E. Efome, D. Rana, T. Matsuura and C. Q. Lan, Metal–organic frameworks supported on nanofiber to remove heavy metals, *J. Mater. Chem. A*, 2018, **6**, 4550–4555.

37 S. Suneesh, R. Kumaresan, S. Rajeswari, P. K. Nayak, *et al.*, Development and Demonstration of Americium (III)-Europium (III) Separation Using Diglycolamic Acid, *Sep. Sci. Technol.*, 2013, **48**, 1998–2006.

38 K. Shimojo, H. Naganawa, J. Noro, F. Kubota, *et al.*, Extraction behavior and separation of lanthanides with a diglycol amic acid derivative and a nitrogen-donor ligand, *Anal. Sci.*, 2007, **23**, 1427–1430.

39 D. Jiang, L. L. Keenan, A. D. Burrowa, *et al.*, Synthesis and post-synthetic modification of MIL-101(Cr)-NH_2 *via* a Tandem diazotization process, *Chem. Commun.*, 2012, **99**, 12053–12055.

40 X. J. Xie, W. Qin, J. W. Wang, X. F. Cui, *et al.*, Leaching of Yttrium and Europium Elements from Waste Fluorescent

Lamps and Kinetics Analysis, *Biolog. Chem. Eng.*, 2021, **5**, 1–6.

41 W. Qin, K. X. Xu, J. W. Wang, X. F. Cui, *et al.*, Phosphorous functionalized PAMAM dendrimers supported on mesoporous silica for Zr(IV) and Hf(IV) separation, *RSC Adv.*, 2021, **11**, 34754–34765.

42 Y. L. Li, Z. T. Xu and W. X. Wang, Effective flocculation of harmful algae Microcystis aeruginosa by nanoscale metal–organic framework NH_2-MIL-101(Cr), *Chem. Eng. J.*, 2022, **433**, 134584–134593.

43 P. Ilaiyaraja, A. K. Singha Deb, D. Ponraju, Sk. Musharaf Al, *et al.*, Surface Engineering of PAMAM-SDB Chelating Resin with Diglycolamic Acid (DGA) Functional Group for Efficient Sorption of U(VI) and Th(IV) from Aqueous Medium, *J. Hazard. Mater.*, 2017, **328**, 1–11.

44 X. L. Zhou, W. Z. Liu, C. Tian, S. Q. Mo, *et al.*, Mussel-inspired functionalization of biological calcium carbonate for improving Eu(III) adsorption and the related mechanisms, *Chem. Eng. J.*, 2018, **351**, 816–824.

45 M. M. Zhang, K. Yang, J. S. Cui, H. B. Yu, *et al.*, 3D-agaric like core-shell architecture UiO-66-NH_2@ZIF-8 with robust stability for highly efficient REEs recovery, *Chem. Eng. J.*, 2020, **386**, 124023–124036.

46 S. P. Ramnani and S. Sabharwal, Adsorption behavior of Cr(VI) onto radiation crosslinked chitosan and its possible application for the treatment of wastewater containing Cr(VI), *React. Funct. Polym.*, 2006, **66**, 902–1002.

47 S. Ryu, C. Fonseka, G. Naidu and P. Loganathan, Recovery of rare earth elements (Lu, Y) by adsorption using functionalized SBA-15 and MIL-101 (Cr), *Chemosphere*, 2021, **281**, 130869–130878.

48 S. Iftekhar, V. Srivastava and M. Sillanpaa, Synthesis and application of LDH intercalated cellulose nanocomposite for separation of rare earth elements (REEs), *Chem. Eng. J.*, 2017, **309**, 130–139.

49 F. Zhao, E. Repo, Y. Meng, X. Wang, D. Yin and M. Sillanpää, An EDTA-b cyclodextrin material for the adsorption of rare earth elements and its application in preconcentration of rare earth elements in seawater, *J. Colloid Interface Sci.*, 2016, **465**, 215–224.

50 Y. R. Lee, K. Yu, S. Ravi and W. S. Ahn, Selective Adsorption of Rare Earth Elements over Functionalized Cr-MIL-101, *ACS Appl. Mater. Interfaces*, 2018, **10**, 23918–23927.

51 X. F. Fang, J. S. Li, X. Li, S. L. Pan and X. Zhang, Internal pore decoration with polydopamine nanoparticle on polymeric ultrafiltration membrane for enhanced heavy metal removal, *Chem. Eng. J.*, 2017, **314**, 38–49.

52 L. Zhang, J. Wang, X. Y. Ren, W. T. Zhang, *et al.*, Internally extended growth of core-shell NH_2-MIL-101(Al)@ZIF-8 nanoflowers for the simultaneous detection and removal of Cu(II), *J. Mater. Chem. A*, 2018, **6**, 21029–21038.